

Spin-Orbit Coupling and Magnetic Anisotropy in Iron-Based Superconductors

Daniel D. Scherer^{*} and Brian M. Andersen[†]

Niels Bohr Institute, University of Copenhagen, Juliane Maries Vej 30, DK-2100 Copenhagen, Denmark



(Received 10 November 2017; published 20 July 2018)

We determine theoretically the effect of spin-orbit coupling on the magnetic excitation spectrum of itinerant multiorbital systems, with specific application to iron-based superconductors. Our microscopic model includes a realistic ten-band kinetic Hamiltonian, atomic spin-orbit coupling, and multiorbital Hubbard interactions. Our results highlight the remarkable variability of the resulting magnetic anisotropy despite constant spin-orbit coupling. At the same time, the magnetic anisotropy exhibits robust universal behavior upon changes in the band structure corresponding to different materials of iron-based superconductors. A natural explanation of the observed universality emerges when considering optimal nesting as a resonance phenomenon. Our theory is also of relevance to other itinerant systems with spin-orbit coupling and nesting tendencies in the band structure.

DOI: 10.1103/PhysRevLett.121.037205

Introduction.—The investigation of magnetism in Fe-based superconducting materials (FeSCs) has proven to be a very rich avenue of research [1]. Symmetry-distinct magnetic phases have been experimentally identified, both collinear and coplanar [2–9], in agreement with theoretical models [10–14]. Recently, it was discovered that distinct collinear phases exhibit completely different orientations of the ordered moments [15], pointing to effects from spin-orbit coupling (SOC). The SOC is typically considered weak in the FeSCs, and hence neglected in many theoretical studies. However, a series of recent observations have reinvigorated the interest in a detailed understanding of SOC and its role in magnetism and superconductivity of these materials. Most prominently, those observations cover details of magnetic anisotropies as seen by polarized neutron scattering [16–18], sizable spin gaps in the ordered states ~ 15 meV [1], as well as considerable SOC-induced band splittings of ~ 10 – 40 meV [19–21], have reinvigorated the interest in a detailed understanding of SOC and its role in magnetism and superconductivity of these materials. In addition, obtaining a quantitative description of the magnetic anisotropy has important implications for the general understanding of the magnetism in terms of mainly localized or itinerant electrons [1,16]. Finally, we note that the importance of SOC has recently been highlighted through the experimental report of topological states and Majorana fermions in a certain class of FeSCs [22,23].

Experimentally, spin-polarized neutron scattering measurements have mapped out the energy (ω) and temperature (T) dependence of the magnetic anisotropy. Below, we denote by M_a , M_b , and M_c the magnetic scattering polarized along the orthorhombic a , b , and c axes, respectively. Focusing first on undoped BaFe_2As_2 , in the magnetic state below T_N the scattering fulfills the hierarchy $M_c > M_b > M_a$. This is in agreement with $\mathbf{Q}_{\text{AF}} = (\pi, 0, \pi)$ ordered moments aligned

antiferromagnetically in the ab plane along the longer a axis, and implies that transverse out-of-plane fluctuations along c are cheaper than in-plane transverse fluctuations in the b direction [1,17,24,25]. The results in the paramagnetic (PM) state at $T > T_N$ at \mathbf{Q}_{AF} can be summarized by the following points: (1) the low-energy magnetic response is isotropic $M_c \approx M_b \approx M_a$ at high T but becomes increasingly anisotropic with $M_a > M_c \gtrsim M_b$ as T approaches T_N [17,24,26]. The fact that M_a is largest agrees with the condensation of moments along the a axis below T_N . (2) This PM magnetic anisotropy close to T_N is observed only at $\omega \lesssim 6$ meV [17]. The doping dependence of the magnetic anisotropy obtained from electron- and hole-doped BaFe_2As_2 [18,26–29], NaFeAs [30], and FeSe [16] has given rise to the following additional points: (3) doping of BaFe_2As_2 tends to enhance the c -axis polarized low-energy magnetic fluctuations in the PM phase such that a range exists where $M_c \gtrsim M_a > M_b$. The enhanced susceptibility along c is consistent with the out-of-plane moment orientation of the C_4 -symmetric magnetic phase observed in Na-doped BaFe_2As_2 [15]. In the nematic PM phase of FeSe , M_c also dominates the inelastic response [16]. (4) At sufficiently large doping (e.g., 15% Ni in BaFe_2As_2), the magnetic anisotropy vanishes [31].

The hierarchy of the magnetic susceptibilities, their ω and T dependence, and their switching as a function of doping has remained an outstanding puzzle, and may naively seem at odds with an atomically defined single-ion spin-orbit-generated magnetic anisotropy. For example, it has been suggested that intervening effects of orbital fluctuations may be at play [17]. Clearly, it is desirable to acquire a microscopic understanding of the interplay between SOC and electronic interactions in the magnetism of FeSCs.

In this Letter, within a realistic ten-band description that properly incorporates atomic SOC, we provide a theoretical

explanation for the above points (1)–(4). We classify the spin-resolved contributions to the particle-hole propagator into different types of excitations. By virtue of SOC, the spin-dependent particle-hole excitations generate a hierarchy in the energy gaps for spin excitations. We propose a general mechanism for the doping dependence of the resulting magnetic anisotropy that turns out to be determined by the position of the optimal nesting of the band on the energy axis and the dominant orbital content of the participating single-particle states. From that perspective, our study is relevant not just to FeSCs, but any itinerant system with SOC and nested bands. Both the T and ω dependence of the anisotropy follow essentially from the smallness of the SOC energy scale together with the enhancement of magnetic scattering close to T - or interaction-driven spin-density wave (SDW) instabilities.

Model.—Upon inclusion of atomic SOC, the itinerant electron system of the FeSC materials is described by a multiorbital Hubbard Hamiltonian $H = H_0 + H_{\text{SOC}} + H_{\text{int}}$ for the electronic degrees of freedom of the $3d$ shell of iron. The noninteracting part describing the electronic structure consists of a hopping Hamiltonian H_0 and an atomic SOC H_{SOC} . We define the fermionic operators $c_{li\mu\sigma}^\dagger$, $c_{li\mu\sigma}$ to create and destroy, respectively, an electron on sublattice l at site i in orbital μ with spin polarization σ . H_0 is written as

$$H_0 = \sum_{\sigma} \sum_{l,l',i,j} \sum_{\mu,\nu} c_{li\mu\sigma}^\dagger (t_{li;l'j}^{\mu\nu} - \mu_0 \delta_{ll'} \delta_{ij} \delta_{\mu\nu}) c_{l'j\nu\sigma}, \quad (1)$$

where hopping matrix elements $t_{li;l'j}^{\mu\nu}$ are material specific and the electronic filling is fixed by the chemical potential μ_0 . The indices $l, l' \in \{A, B\}$ denote the 2-Fe sublattices, corresponding to the two inequivalent Fe sites in the 2-Fe unit cell due to the pnictogen (Pn)/chalcogen (Ch) staggering about the FePn/FeCh plane. The orbital indices μ, ν label the five $3d$ orbitals at a given Fe site. In a suitable chosen (phase-staggered) basis, see Supplemental Material [32], the atomic SOC Hamiltonian reads as

$$H_{\text{SOC}} = \frac{\lambda}{2} \sum_{l,i} \sum_{\mu,\nu} \sum_{\sigma,\sigma'} c_{li\mu\sigma}^\dagger [\mathbf{L}_l]_{\mu\nu} \cdot \boldsymbol{\sigma}_{\sigma\sigma'} c_{liv\sigma'}. \quad (2)$$

Electronic interactions of the $3d$ states are modeled by a local Hubbard-Hund interaction term

$$H_{\text{int}} = U \sum_{l,i,\mu} n_{li\mu\uparrow} n_{li\mu\downarrow} + \left(U' - \frac{J}{2} \right) \sum_{l,i,\mu < \nu, \sigma, \sigma'} n_{li\mu\sigma} n_{liv\sigma'} - 2J \sum_{l,i,\mu < \nu} \mathbf{S}_{li\mu} \cdot \mathbf{S}_{liv} + J' \sum_{l,i,\mu < \nu, \sigma} c_{li\mu\sigma}^\dagger c_{liv\sigma}^\dagger c_{liv\sigma} c_{li\mu\sigma}, \quad (3)$$

parametrized by an intraorbital Hubbard U , an interorbital coupling U' , Hund's coupling J and pair hopping J' , satisfying $U' = U - 2J$, $J = J'$. The operators for local

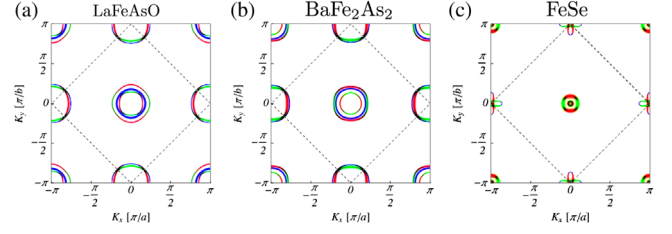


FIG. 1. Fermi surfaces in the 1-Fe BZ [(K_x, K_y) denotes momenta in the 1-Fe BZ coordinate system] extracted from the orbitally resolved electronic spectral function with $\mu_0 = 0$ eV and $\lambda = 0.025$ eV for (a) LaFeAsO, (b) BaFe₂As₂, and (c) FeSe. The dashed square denotes the 2-Fe BZ. The green and red parts of the Fermi surfaces are dominated by yz and xz orbitals, respectively, while blue corresponds to xy . The contribution of $x^2 - y^2$ and $3z^2 - r^2$ orbitals to the spectral weight at the Fermi level is negligible.

charge and spin are $n_{li\mu} = n_{li\mu\uparrow} + n_{li\mu\downarrow}$ with $n_{li\mu\sigma} = c_{li\mu\sigma}^\dagger c_{li\mu\sigma}$ and $\mathbf{S}_{li\mu} = 1/2 \sum_{\sigma\sigma'} c_{li\mu\sigma}^\dagger \boldsymbol{\sigma}_{\sigma\sigma'} c_{li\mu\sigma'}$, respectively.

Below, we will consider three sets of hopping parameters $t_{li;l'j}^{\mu\nu}$ for different FeSC parent materials taken from the DFT literature: LaFeAsO [33], BaFe₂As₂ [34], and FeSe [35], see Fig. 1 for the corresponding orbitally resolved Fermi surfaces with finite SOC. All three Fermi surfaces display approximate nesting with nesting vector \mathbf{Q}_{AF} between the hole pockets at the center and the electron pockets at the boundary of the BZ. The FeSe-Fermi surface, see Fig. 1(c), deviates strongly from typical FeSC Fermi surfaces. We have modeled the FeSe Fermi surface by including a self-consistent nearest-neighbor hopping renormalization [35]. The effect of hole or electron doping is obtained by a rigid shift in the chemical potential μ_0 . As to the choice of SOC values, we limit ourselves to values producing splittings in the ~ 10 meV range in the electronic spectrum, as observed by angle-resolved photoemission spectroscopy. When discussing interaction effects for BaFe₂As₂, the values of U and J are chosen to bring the undoped ($\mu_0 = 0$ eV) system close to an SDW instability, where the enhancement of the anisotropy by interactions becomes most pronounced.

For further details on the band structures and the effects of SOC, we refer to the Supplemental Material [32].

Spin susceptibility.—To make connection to neutron scattering, we compute the imaginary-time spin-spin correlation function (here i, j refer to the spatial directions x, y, z)

$$\chi^{ij}(i\omega_n, \mathbf{q}) = \frac{g^2}{2} \int_0^\beta d\tau e^{i\omega_n \tau} \langle \mathcal{T}_\tau S_{\mathbf{q}}^i(\tau) S_{-\mathbf{q}}^j(0) \rangle, \quad (4)$$

with $g = 2$ and the Fourier transformed electron spin operator for the 2-Fe unit cell given as

$$S_{\mathbf{q}}^i(\tau) = \frac{1}{\sqrt{\mathcal{N}}} \sum_{\mathbf{k}, l, \mu, \sigma, \sigma'} c_{\mathbf{k}-\mathbf{q}l\mu\sigma}^\dagger(\tau) \frac{\sigma_{\sigma\sigma'}^i}{2} c_{\mathbf{k}l\mu\sigma'}(\tau). \quad (5)$$

To account for interaction effects in the weak-coupling regime, we evaluate the correlation functions in the random-phase approximation (RPA) in the absence of spin-rotation invariance, see Supplemental Material [32]. Performing analytic continuation $i\omega_n \rightarrow \omega + i\eta$, with $\eta > 0$ a small smearing parameter, we gain access to the momentum- and frequency-resolved spectral density of magnetic excitations with different spatial polarizations probed by polarized neutron scattering. We have $M_i(\omega) \sim \text{Im}[\chi^{ii}(\omega + i\eta, \mathbf{Q}_{\text{AF}})]$, in a coordinate system $x = a$, $y = b$, $z = c$ aligned with the orthorhombic crystal axes and $\mathbf{Q}_{\text{AF}} = \mathbf{Q}_{1,2}$ with the nesting vectors $\mathbf{Q}_1 = (\pi, 0)$, $\mathbf{Q}_2 = (0, \pi)$, where \mathbf{Q}_2 is related to \mathbf{Q}_1 by a C_4 rotation in the ab plane. The cross terms with $i \neq j$ vanish for the commensurate wave vector \mathbf{Q}_{AF} .

Since the interaction term H_{int} is rotationally symmetric, it cannot create anisotropy in the magnetic response. Hence, all SOC-driven anisotropy is contained purely in the particle-hole propagator, and therefore the origin of anisotropy is found in the structure of the noninteracting susceptibility. In terms of the sublattice-, orbital-, and spin-resolved electronic Greens function, the noninteracting susceptibility reads

$$\chi_0^{ij}(q) = \frac{1}{2} \sum_{\sigma_1 \dots \sigma_4} \sigma_{\sigma_1 \sigma_2}^i \sigma_{\sigma_3 \sigma_4}^j G_{\sigma_2 \sigma_3} G_{\sigma_4 \sigma_1}, \quad (6)$$

where for compact notation we defined

$$G_{\sigma_2 \sigma_3} G_{\sigma_4 \sigma_1} \equiv -\frac{g^2}{4\beta\mathcal{N}} \sum G_{l\mu\sigma_2;l'\nu\sigma_3}(k) G_{l'\nu\sigma_4;l\mu\sigma_1}(k-q),$$

with $q = (i\omega_n, \mathbf{q})$ and $k = (i\nu_p, \mathbf{k})$, $i\omega_n$, $i\nu_p$ being bosonic and fermionic Matsubara frequencies, respectively, and the shorthand $\sum(\dots) = \sum_k \sum_{l,l'} \sum_{\mu,\nu}(\dots)$. According to Eq. (6), the susceptibility can be decomposed into its orbital contributions as $\chi_0^{ij}(q) = \sum_{\mu,\nu} [\chi_0^{ij}(q)]^{\mu,\nu}$. Performing the Matsubara sum yields a Lindhard factor dressed by wave vector-dependent matrix elements, see Supplemental Material [32]. We can then extract the isotropic contribution to the susceptibility as $\chi_0 = \frac{1}{4} \sum_{\sigma} [G_{\sigma\sigma} G_{\sigma\sigma} + G_{\sigma\sigma} G_{\bar{\sigma}\bar{\sigma}}]$. The anisotropic contributions, $\Delta\chi_0^{ii} = \chi_0^{ii} - \chi_0$, can be expressed in terms of three particle-hole amplitudes $\Delta\chi_0^{xx} = \psi^{++} - \phi$, $\Delta\chi_0^{yy} = -\psi^{++} - \phi$, $\Delta\chi_0^{zz} = -\psi^{+-} + \phi$, where we have defined the summed amplitudes $\psi^{++} = \frac{1}{2} \sum_{\sigma} G_{\sigma\bar{\sigma}} G_{\sigma\bar{\sigma}}$, $\psi^{+-} = \frac{1}{2} \sum_{\sigma} G_{\sigma\bar{\sigma}} G_{\bar{\sigma}\sigma}$, $\phi = \frac{1}{4} \sum_{\sigma} [G_{\sigma\sigma} G_{\sigma\sigma} - G_{\sigma\sigma} G_{\bar{\sigma}\bar{\sigma}}]$.

In the non-nematic PM state, the anisotropic response at \mathbf{Q}_2 is related to that at \mathbf{Q}_1 by a C_4 transformation about the c axis: $\Delta\chi_0^{xx/yy}(\mathbf{Q}_2) = \Delta\chi_0^{yy/xx}(\mathbf{Q}_1)$ and $\Delta\chi_0^{zz}(\mathbf{Q}_2) = \Delta\chi_0^{zz}(\mathbf{Q}_1)$. The amplitude ϕ , measuring the difference of equal- and opposite-spin (with respect to the z axis pointing out of plane) particle-hole propagation is insensitive to a C_4 rotation. Likewise, the amplitude ψ^{+-} corresponds to processes that are possible due to SOC, but do not change the total spin along the z direction. In contrast, the spin-flip

amplitude ψ^{++} , where both electron and hole with a fixed initial spin propagate to the opposite spin state by virtue of SOC, reacts by a sign change. A commonality between the bands is the sublattice structure of the anisotropy-generating particle-hole amplitudes. While ψ^{++} receives only intersublattice contributions, ψ^{+-} and ϕ only come from intrasublattice terms.

The physical interpretation of the particle-hole bubble diagrams can be made more transparent by considering SOC within perturbation theory. We find that the leading contribution to the anisotropy at \mathbf{Q}_{AF} emerges at order λ^2 (see Supplemental Material [32] for details). This is in contrast to previous work [36], where the leading anisotropy was found to be of the form $J\lambda^2$ and depended crucially on a finite Hund's coupling. We additionally investigated the importance of the sign of λ , see Supplemental Material [32], and found that results for the magnetic anisotropy are only weakly affected.

Anisotropy without interactions.—Our findings for the doping dependence of the magnetic anisotropy for the noninteracting LaFeAsO, BaFe₂As₂, and FeSe models at $k_B T = 0.01$ eV are shown in Fig. 2 for several values of λ . For the 1111 and 122 bands, there exists a clear correlation between the position of the optimal nesting condition on the energy axis (that is only weakly dependent on small λ), see Figs. 2(a) and 2(b), and the central peak in the static anisotropic response as a function of μ_0 , seen in Figs. 2(d) and 2(e). Indeed, the characteristic μ_0 dependence of the anisotropy can be qualitatively reproduced in a simple level model, see Supplemental Material [32], where the optimal nesting condition is replaced by isolated levels with xy and yz orbital content, coupled by SOC. This simple model also provides the same type of spin-dependent particle-hole amplitudes as seen in the tight-binding models, cf. Figs. 2(g) and 2(h), pointing to a universal mechanism behind the doping dependence of the magnetic anisotropy across the FeSC materials. In this picture the behavior of $\Delta\chi_0^{ii}$ with doping is determined largely by the position of the optimal nesting condition on the energy axis and the symmetry properties of the participating orbitals.

For all three tight-binding models, the hierarchy in the magnetic anisotropy changes with μ_0 . While the different realizations of the hierarchy are already apparent at $\lambda = 0.015$ eV, increasing λ enlarges the doping range with a particular form of the hierarchy. For LaFeAsO and BaFe₂As₂ we obtain a dominating χ_0^{xx} in the undoped case, while on the hole-(electron-)doped side, an extended region with dominating χ_0^{zz} (χ_0^{yy}) exists. Sufficiently far away from the nesting resonance, the magnetic anisotropy drops rapidly. These findings are in excellent agreement with properties (3) and (4) highlighted in the introduction. The most prominent difference in the doping dependence occurs on the hole-doped side, where $\Delta\chi_0^{xx}$ and $\Delta\chi_0^{yy}$ in the LaFeAsO and FeSe models do not display zero crossings, as opposed to the BaFe₂As₂ case. In addition, the FeSe

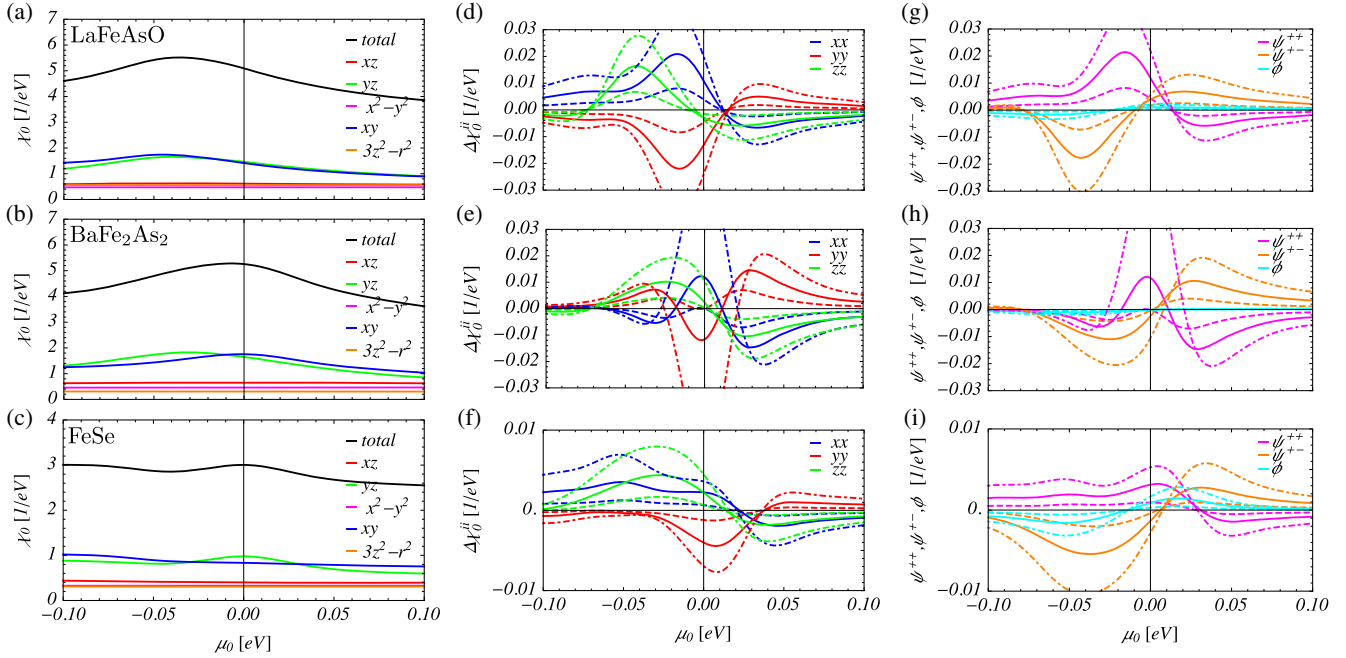


FIG. 2. (a)–(c) Chemical potential dependence of the total and orbitally ($\mu = \nu$ only) resolved isotropic contribution to the static noninteracting susceptibility with SOC $\lambda = 0.025$ eV at $k_B T = 0.01$ eV for the (a) LaFeAsO, (b) BaFe₂As₂, and (c) FeSe model with fixed wave vector \mathbf{Q}_1 . (d)–(f) Corresponding anisotropic contributions and (g)–(i) summed particle-hole amplitudes contributing to the anisotropic magnetic response for $\lambda = 0.015$ eV (dashed), $\lambda = 0.025$ eV (solid) and $\lambda = 0.035$ eV (dot-dashed).

model, where optimal nesting for xy and yz orbitals is weakened and occurs in different places on the μ_0 axis, see Fig. 2(c), displays a dominating χ_0^{zz} in the undoped case for sufficiently large λ . This agrees with the recent findings in Ref. [16], see Fig. 2(f). Both weak hole doping or increasing λ enhance the dominance of out-of-plane spin-fluctuations compared to in-plane fluctuations. The anisotropy is driven by the same type of particle-hole excitations in all models, cf. Figs. 2(g)–2(i). Only ψ^{++} and ψ^{+-} yield sizable contributions in the LaFeAsO and BaFe₂As₂ bands, with ϕ basically vanishing. For FeSe the ϕ amplitude is stronger compared to the 1111 and 122 cases.

Anisotropy with interactions.—The static bare susceptibility provides us with a measure of the gap sizes of spin excitations with different polarization. We can, thus, qualitatively connect the results in Fig. 2 to the doping dependence of the magnetic scattering amplitudes M_i . We note that we do not expect the RPA (neglecting self-energy and vertex corrections) to yield quantitative results in terms of absolute magnitudes of the scattering amplitudes. It is known that a pure RPA-type quasiparticle calculation yields too small scattering intensities. There is evidence, however, that in correlated systems with well-defined quasiparticles, the inclusion of vertex corrections mainly shifts the quasiparticle result to realistic amplitudes [37]. Focusing on BaFe₂As₂, cf. Fig. 2(e), our weak-coupling approach yields $M_a > M_c > M_b$ in an extended region around $\mu_0 = 0$ eV, consistent with a stripe SDW state with

ordered moments along a . The formation of a finite SDW order below T_N results in the gapping of excitations parallel to the moment direction. For sufficiently low T in the stripe magnetic state, we can thus expect $M_c > M_b > M_a$. Returning to the discussion of the PM state, for sufficiently strong SOC, hole doping first leads to a regime with $M_c > M_a > M_b$, with a subsequent crossover to $M_c > M_b > M_a$ upon further hole doping, all consistent with the observed reorientation of magnetic moments in a C_4 -symmetric magnetic phase [15].

We show the ω -dependent RPA results for the imaginary part of the susceptibility in the various regimes in Fig. 3(a) for interaction parameters U and J close to the interaction driven SDW instability with fixed wave vector. For the undoped case ($\mu_0 = 0$ eV) the ω -dependent anisotropy in the magnetic scattering is clearly visible and diminishes quickly for $\omega \gtrsim 6$ –7 meV. In the hole- ($\mu = -0.05$ eV) and electron-doped ($\mu = 0.05$ eV) cases, the changes in the hierarchy of magnetic scattering can be observed with an overall decrease of the magnetic scattering, while at the same time the anisotropy appears over a larger energy range. These differences to the undoped case are simply due to the increasing degree of incommensurability of the wave vector associated with the leading SDW instability, while we observe the magnetic scattering at the commensurate wave vector \mathbf{Q}_{AF} . Thus, the magnetic excitations at \mathbf{Q}_{AF} obtain larger gaps for the doped cases than for the undoped case shown in Fig. 3(a). The T dependence of $\text{Re}[\chi^{ii}(0 + i\eta, \mathbf{Q}_{AF})]$ is shown in Fig. 3(b), where χ^{xx}

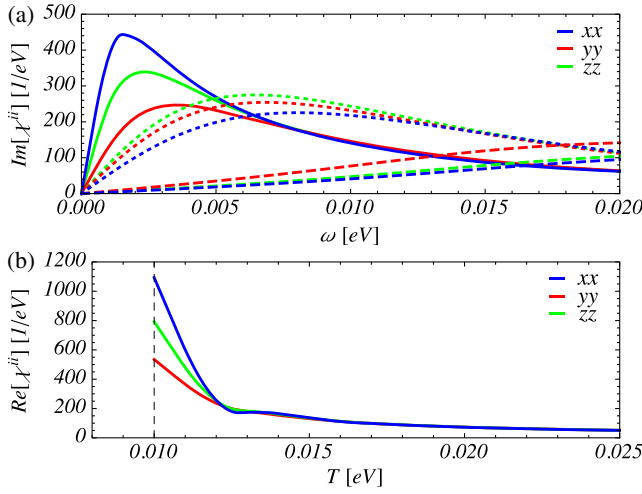


FIG. 3. (a) Imaginary part of the interacting susceptibilities as a function of ω at wave vector \mathbf{Q}_1 for the BaFe₂As₂ model with $\lambda = 0.025$ eV at $k_B T = 0.01$ eV close to the interaction driven SDW instability (with $J = U/4$) for different chemical potentials: $\mu_0 = 0$ eV, $U = 0.815$ eV (solid), $\mu_0 = -0.05$ eV, $U = 0.898$ eV (dotted), and $\mu_0 = 0.05$ eV, $U = 1.030$ eV (dashed). (b) T dependence of the static part of the RPA susceptibility for $\mu_0 = 0$ eV with $\lambda = 0.025$ eV and $U = 0.816$ eV, $J = U/4$. The dashed vertical line marks the SDW transition temperature T_N .

diverges as $T \rightarrow T_N$. The anisotropy increases strongly in the proximity to the SDW transition, while it remains small for elevated T . The results shown in Fig. 3 are in excellent agreement with the points (1) and (2) discussed in the introduction. Thus, we conclude that the model approach presented here seems to adequately describe the magnetic anisotropy of FeSCs. Interesting future studies include calculations of $\chi^{ii}(q)$ in the presence of SOC in the superconducting state where magnetic anisotropy of the neutron resonance has been reported by polarized neutron scattering [16,18,26,38–41].

We acknowledge discussions with M. H. Christensen, P. Dai, I. Eremin, A. Kreisler, and F. Lambert, and financial support from the Carlsberg Foundation.

*daniel.scherer@nbi.ku.dk

†bma@nbi.ku.dk

- [1] P. Dai, *Rev. Mod. Phys.* **87**, 855 (2015).
- [2] S. Avci, O. Chmaissem, J. M. Allred, S. Rosenkranz, I. Eremin, A. V. Chubukov, D. E. Bugaris, D. Y. Chung, M. G. Kanatzidis, J.-P. Castellan, J. A. Schlueter, H. Claus, D. D. Khalyavin, P. Manuel, A. Daoud-Aladine, and R. Osborn, *Nat. Commun.* **5**, 3845 (2014).
- [3] A. E. Böhmer, F. Hardy, L. Wang, T. Wolf, P. Schweiss, and C. Meingast, *Nat. Commun.* **6**, 7911 (2015).
- [4] J. M. Allred, S. Avci, D. Y. Chung, H. Claus, D. D. Khalyavin, P. Manuel, K. M. Taddei, M. G. Kanatzidis, S. Rosenkranz, R. Osborn, and O. Chmaissem, *Phys. Rev. B* **92**, 094515 (2015).

- [5] Y. Zheng, P. M. Tam, J. Hou, A. E. Böhmer, T. Wolf, C. Meingast, and R. Lortz, *Phys. Rev. B* **93**, 104516 (2016).
- [6] B. P. P. Mallett, Y. G. Pashkevich, A. Gusev, T. Wolf, and C. Bernhard, *Euro. Phys. Lett.* **111**, 57001 (2015).
- [7] B. P. P. Mallett, P. Marsik, M. Yazdi-Rizi, T. Wolf, A. E. Böhmer, F. Hardy, C. Meingast, D. Munzar, and C. Bernhard, *Phys. Rev. Lett.* **115**, 027003 (2015).
- [8] J. M. Allred, K. M. Taddei, D. E. Bugaris, M. J. Krogstad, S. H. Lapidus, D. Y. Chung, H. Claus, M. G. Kanatzidis, D. E. Brown, J. Kang, R. M. Fernandes, I. Eremin, S. Rosenkranz, O. Chmaissem, and R. Osborn, *Nat. Phys.* **12**, 493 (2016).
- [9] W. R. Meier, Q.-P. Ding, A. Kreyssig, S. L. Bud'ko, A. Sapkota, K. Kothapalli, V. Borisov, R. Valentí, C. D. Batista, P. P. Orth, R. M. Fernandes, A. I. Goldman, Y. Furukawa, A. E. Böhmer, and P. C. Canfield, *npj Quantum Mater.* **3**, 5 (2018).
- [10] J. Lorenzana, G. Seibold, C. Ortix, and M. Grilli, *Phys. Rev. Lett.* **101**, 186402 (2008).
- [11] I. Eremin and A. V. Chubukov, *Phys. Rev. B* **81**, 024511 (2010).
- [12] M. N. Gastiasoro and B. M. Andersen, *Phys. Rev. B* **92**, 140506(R) (2015).
- [13] D. D. Scherer, I. Eremin, and B. M. Andersen, *Phys. Rev. B* **94**, 180405(R) (2016).
- [14] M. H. Christensen, D. D. Scherer, P. Kotetes, and B. M. Andersen, *Phys. Rev. B* **96**, 014523 (2017).
- [15] F. Waßer, A. Schneidewind, Y. Sidis, S. Wurmehl, S. Aswartham, B. Büchner, and M. Braden, *Phys. Rev. B* **91**, 060505(R) (2015).
- [16] M. Ma, P. Bourges, Y. Sidis, Y. Xu, S. Li, B. Hu, J. Li, F. Wang, and Y. Li, *Phys. Rev. X* **7**, 021025 (2017).
- [17] Y. Li, W. Wang, Y. Song, H. Man, X. Lu, F. Bourdarot, and P. Dai, *Phys. Rev. B* **96**, 020404(R) (2017).
- [18] Y. Song, H. R. Man, R. Zhang, X. Y. Lu, C. L. Zhang, M. Wang, G. T. Tan, L.-P. Regnault, Y. X. Su, J. Kang, R. M. Fernandes, and P. C. Dai, *Phys. Rev. B* **94**, 214516 (2016).
- [19] P. D. Johnson, H.-B. Yang, J. D. Rameau, G. D. Gu, Z.-H. Pan, T. Valla, M. Weinert, and A. V. Fedorov, *Phys. Rev. Lett.* **114**, 167001 (2015).
- [20] M. D. Watson, T. K. Kim, A. A. Haghighirad, N. R. Davies, A. McCollam, A. Narayanan, S. F. Blake, Y. L. Chen, S. Ghannadzadeh, A. J. Schofield, M. Hoesch, C. Meingast, T. Wolf, and A. I. Coldea, *Phys. Rev. B* **91**, 155106 (2015).
- [21] S. V. Borisenko, D. V. Evtushinsky, Z.-H. Liu, I. Morozov, R. Kappenberger, S. Wurmehl, B. Büchner, A. N. Yaresko, T. K. Kim, M. Hoesch, T. Wolf, and N. D. Zhigadlo, *Nat. Phys.* **12**, 311 (2016).
- [22] P. Zhang, K. Yaji, T. Hashimoto, Y. Ota, T. Kondo, K. Okazaki, Z. Wang, J. Wen, G. D. Gu, H. Ding, and S. Shin, *Science* **360**, 182 (2018).
- [23] D. Wang, L. Kong, P. Fan, H. Chen, Y. Sun, S. Du, J. Schneeloch, R. D. Zhong, G. D. Gu, L. Fu, H. Ding, and H. Gao, *arXiv:1706.06074*.
- [24] N. Qureshi, P. Steffens, S. Wurmehl, S. Aswartham, B. Büchner, and M. Braden, *Phys. Rev. B* **86**, 060410(R) (2012).
- [25] C. Wang, R. Zhang, F. Wang, H. Luo, L. P. Regnault, P. Dai, and Y. Li, *Phys. Rev. X* **3**, 041036 (2013).
- [26] H. Luo, M. Wang, C. Zhang, X. Lu, L.-P. Regnault, R. Zhang, S. Li, J. Hu, and P. Dai, *Phys. Rev. Lett.* **111**, 107006 (2013).

- [27] C. Zhang, M. Liu, Y. Su, L.-P. Regnault, M. Wang, G. Tan, Th. Brückel, T. Egami, and P. Dai, *Phys. Rev. B* **87**, 081101 (2013).
- [28] N. Qureshi, C. H. Lee, K. Kihou, K. Schmalzl, P. Steffens, and M. Braden, *Phys. Rev. B* **90**, 100502 (2014).
- [29] K. Matano, Z. Li, G. L. Sun, D. L. Sun, C. T. Lin, M. Ichioka, and G. Zheng, *Europhys. Lett.* **87**, 27012 (2009).
- [30] Y. Song, L.-P. Regnault, C. Zhang, G. Tan, S. V. Carr, S. Chi, A. D. Christianson, T. Xiang, and P. Dai, *Phys. Rev. B* **88**, 134512 (2013).
- [31] M. Liu, C. Lester, J. Kulda, X. Lu, H. Luo, M. Wang, S. M. Hayden, and P. Dai, *Phys. Rev. B* **85**, 214516 (2012).
- [32] See Supplemental Material at <http://link.aps.org/supplemental/10.1103/PhysRevLett.121.037205> for details on the S1. Effect of $\text{sgn}(\lambda)$ on electronic bandstructure and anisotropy, S2. RPA correlation functions, S3. Second-order perturbation theory in spin-orbit coupling and a simple, and S4. Fermionic level model, that illustrates the universal features of the anisotropic magnetic response.
- [33] H. Ikeda, R. Arita, and J. Kuneš, *Phys. Rev. B* **81**, 054502 (2010).
- [34] H. Eschrig and K. Koepf, *Phys. Rev. B* **80**, 104503 (2009).
- [35] D. D. Scherer, A. C. Jacko, C. Friedrich, E. Şaşıoğlu, S. Blügel, R. Valentí, and B. M. Andersen, *Phys. Rev. B* **95**, 094504 (2017).
- [36] M. H. Christensen, J. Kang, B. M. Andersen, I. Eremin, and R. M. Fernandes, *Phys. Rev. B* **92**, 214509 (2015).
- [37] E. A. Goremychkin, H. Park, R. Osborn, S. Rosenkranz, J.-P. Castellán, V. R. Fanelli, A. D. Christianson, M. B. Stone, E. D. Bauer, K. J. McClellan, D. D. Byler, and J. M. Lawrence, *Science* **359**, 186 (2018).
- [38] O. J. Lipscombe, L. W. Harriger, P. G. Freeman, M. Enderle, C. Zhang, M. Wang, T. Egami, J. Hu, T. Xiang, M. R. Norman, and P. Dai, *Phys. Rev. B* **82**, 064515 (2010).
- [39] P. Steffens, C. H. Lee, N. Qureshi, K. Kihou, A. Iyo, H. Eisaki, and M. Braden, *Phys. Rev. Lett.* **110**, 137001 (2013).
- [40] C. Zhang, Y. Song, L.-P. Regnault, Y. Su, M. Enderle, J. Kulda, G. Tan, Z. C. Sims, T. Egami, Q. Si, and P. Dai, *Phys. Rev. B* **90**, 140502(R) (2014).
- [41] F. Waßer, C. H. Lee, K. Kihou, P. Steffens, K. Schmalzl, N. Qureshi, and M. Braden, *Sci. Rep.* **7**, 10307 (2017).